Parthenolide-induced apoptosis of hepatic stellate cells and anti-fibrotic effects in an *in vivo* rat model

In Hee Kim[1], Sang Wook Kim[1], Seong Hun Kim[1], Seung Ok Lee[1], Soo Teik Lee[1], Dae-Ghon Kim[1,3], Mi-Jin Lee[1] and Woo Hyun Park[2]

[1]Department of Internal Medicine
Research Institute of Clinical Medicine
Chonbuk National University Medical School and Hospital
Jeonju 561-712, Korea
[2]Department of Physiology
Chonbuk National University Medical School
Jeonju 561-712, Korea
[3]Corresponding author: Tel, 82-63-251-1681;
Fax, 82-63-254-1609; E-mail, daeghon@jbnu.ac.kr
http://dx.doi.org/10.3858/emm.2012.44.7.051

Abstract

Parthenolide (PT), a sesquiterpene lactone derived from the plant feverfew, has pro-apoptotic activity in a number of cancer cell types. We assessed whether PT induces the apoptosis of hepatic stellate cells (HCSs) and examined its effects on hepatic fibrosis in an *in vivo* model. The effects of PT on rat HSCs were investigated in relation to cell growth inhibition, apoptosis, NF-κB binding activity, intracellular reactive oxygen species (ROS) generation, and glutathione (GSH) levels. In addition, the anti-fibrotic effects of PT were investigated in a thioacetamide-treated rat model. PT induced growth inhibition and apoptosis in HSCs, as evidenced by cell growth inhibition and apoptosis assays. PT increased the expression of Bax proteins during apoptosis, but decreased the expression of Bcl-2 and Bcl-X$_L$ proteins. PT also induced a reduction in mitochondrial membrane potential, poly(ADP-ribose) polymerase cleavage, and caspase-3 activation. PT inhibited TNF-α-stimulated NF-κB binding activity in HSCs. The pro-apoptotic activity of PT in HSCs was associated with increased intracellular oxidative stress as evidenced by increased intracellular ROS levels and depleted intracellular GSH levels. Furthermore, PT ameliorated hepatic fibrosis significantly in a thioacetamide-treated rat model. In conclusion, PT exhibited pro-apoptotic effects in rat HSCs and ameliorated hepatic fibrosis in a thioacetamide-induced rat model.

Keywords: apoptosis; hepatic stellate cells; liver cirrhosis; parthenolide; reactive oxygen species; thioacetamide

Introduction

The key cellular process of hepatic fibrosis is the activation and phenotypic change of hepatic stellate cells (HSCs) into proliferative, contractile, and chemotactic myofibroblasts producing extracellular matrix (Friedman, 2000). The transdifferentiation process of HSCs into myofibroblasts involves expression of α-smooth muscle actin (α-SMA). Increasing evidence suggests that hepatic fibrosis is reversible, and the discovery that the reversion of fibrosis is accompanied by the clearance of HSCs by apoptosis is a key piece of this evidence (Iredale *et al.*, 1998; Arthur, 2002). Experimental augmentation of HSC apoptosis reduces hepatic fibrosis, thereby confirming the notion that HSC apoptosis can be used as a therapeutic anti-fibrogenic strategy (Elsharkawy *et al.*, 2005).

Parthenolide (PT) is a sesquiterpene lactone derived from the plant feverfew (*Tanacetum parthenium*), which is used in folk medicine to treat various inflammatory conditions such as rheumatoid arthritis, fever, and migraine (Schinella *et al.*, 1998). PT contains an α-methylene-γ-lactone ring and an epoxide, which interact readily with nucleophilic sites in biological molecules. Modern scientific studies have revealed that PT has anti-microbial, anti-inflammatory, and anti-cancer properties (Hehner *et al.*, 1998; Schinella *et al.*, 1998; Pajak *et al.*, 2008). Furthermore, PT has been shown to promote cellular differentiation, cause cells to exit the cell

cycle, and induce apoptosis. PT has also been shown to inhibit nuclear factor kappa B (NF-κB)-mediated anti-apoptotic transcription and to have a strong pro-apoptotic effect on cancer cells by stimulating the intrinsic apoptotic pathway which involves elevated levels of intracellular reactive oxygen species (ROS) and modifications of Bcl-2 family proteins (Wen *et al.*, 2002; Zhang *et al.*, 2004b; Wang *et al.*, 2006). HSC activation is associated with activation of NF-κB, a potent pro-survival transcription factor. Several studies have indicated that NF-κB inhibition provides a potent means of inducing HSC apoptosis (Habens *et al.*, 2005; Oakley *et al.*, 2005). In a previous study, inhibition of NF-κB by pretreatment with PT increased the extent of apoptotic death of HCS induced by 3,4-methylenedioxymethamphetamine (Montiel-Duarte *et al.*, 2004). However, the latter study has not examined the further apoptotic effect or the mechanism of PT on HSCs, and there was no report on the anti-fibrotic effect of PT *in vivo*.

In the present study, we investigated the pro-apoptotic effect of PT on rat HSCs and the mechanism of PT *in vitro*. In addition, we evaluated the anti-fibrotic effect of PT using a thioacetamide (TAA)-induced *in vivo* rat model.

Results

Anti-proliferative and pro-apoptotic effects of PT in rat HSCs

Phase contrast microscopy of RI-T cells after treatment with PT showed striking morphologic alterations. The phenotype of RI-T cells changed from a flattened, fibroblastic morphology with distinct cell-cell interfaces to a substratum-detached, rounded, and blebbed morphology (Figure 1A). After exposure to PT for 24 h, RI-T cell growth was dose-dependently inhibited (Figure 1B). PT increased the sub-G1 population in a dose-dependent manner at 24 h (Figure 1C). As was observed for percentages of sub-G1 group cells as determined by flow cytometry, the proportion of annexin V-stained cells among PT-treated cells increased in a dose-dependent manner (Figure 1D), which supports the notion that PT-induced RI-T cell death occurs *via* apoptosis.

Susceptibility of hepatic HSCs to PT-induced apoptosis

Susceptibility of rat HSCs to PT-induced apoptosis was significantly higher than that of rat hepatocytes (Figure 2A). Accordingly, cleavage of caspase-3 and PARP, indicators of apoptotic cell death, was more prominent in HSCs than in hepatocytes (Figure 2B). To determine whether NF-κB DNA binding activity is blocked by PT in RI-T cells, we studied the effect of PT on the TNF-α-stimulated translocation of NF-κB from the cytoplasmic compartment to the nucleus and the effect on NF-κB DNA binding activity in RI-T cells (Figure 2C). TNF-α (10 ng/ml)-stimulated RI-T cells showed greater DNA binding activity by a NF-κB consensus sequence as compared with unstimulated cells. In
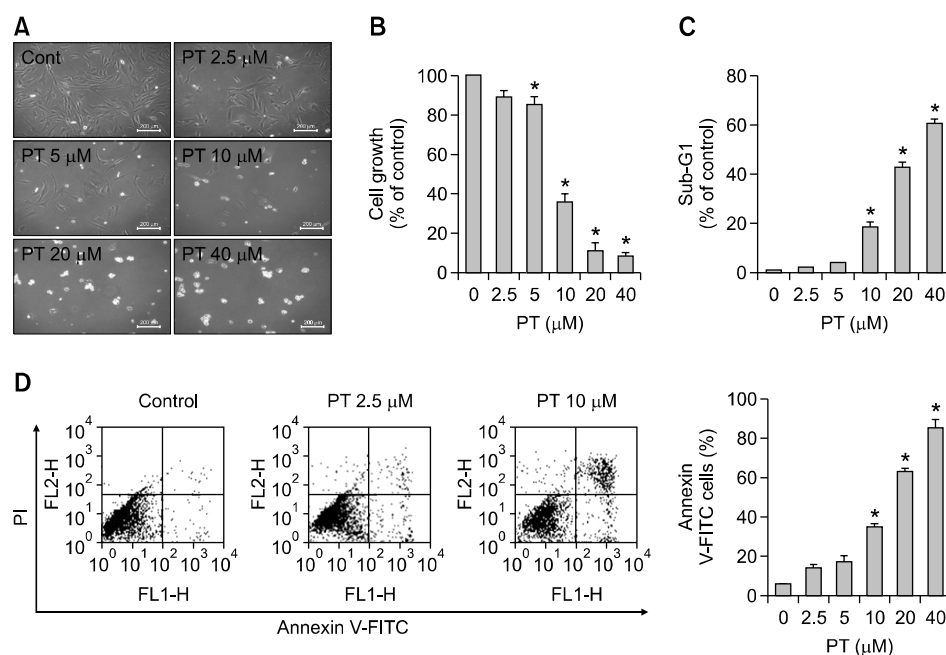

Figure 1. PT inhibits the growth of RI-T cells. (A) Phase contrast microscopic photographs (magnification ×100) in PT-treated RI-T cells. (B) Cell growth inhibition was assessed using MTT assays. (C) Sub-G1 cell percentages were measured by DNA flow cytometric analysis. (D) Cells with annexin V staining were counted using a FACStar flow cytometer (left). The graph shows percentages of annexin-V-positive cells (right). *$P < 0.05$ for the PT-treated group versus the untreated control group.

addition, TNF-α-stimulated NF-κB binding activity was found to be suppressed significantly by pretreatment with PT at 10-20 µM. Furthermore, pyrrolidinedithiocarbamate (PDTC), another well known NF-κB inhibitor, also induced apoptotic cell death, which was reduced by TNF-α-stimulation (Figure 2D). However, the additional effect of PT and PDTC on apoptotic cell death was not clear.

Changes in apoptosis-related proteins and MMP during PT-induced apoptosis of rat HSCs

To investigate the mechanism of PT-induced apoptosis of RI-T cells, the effect of PT on Bcl-2 family proteins during apoptosis was determined. We observed that Bcl-X$_L$ and Bcl-2 protein levels were decreased, whereas Bax protein levels were increased. We also examined the effect of PT on the cleavage of their substrate, PARP, and on the activation of caspase-3. Cleavage and/or reduction
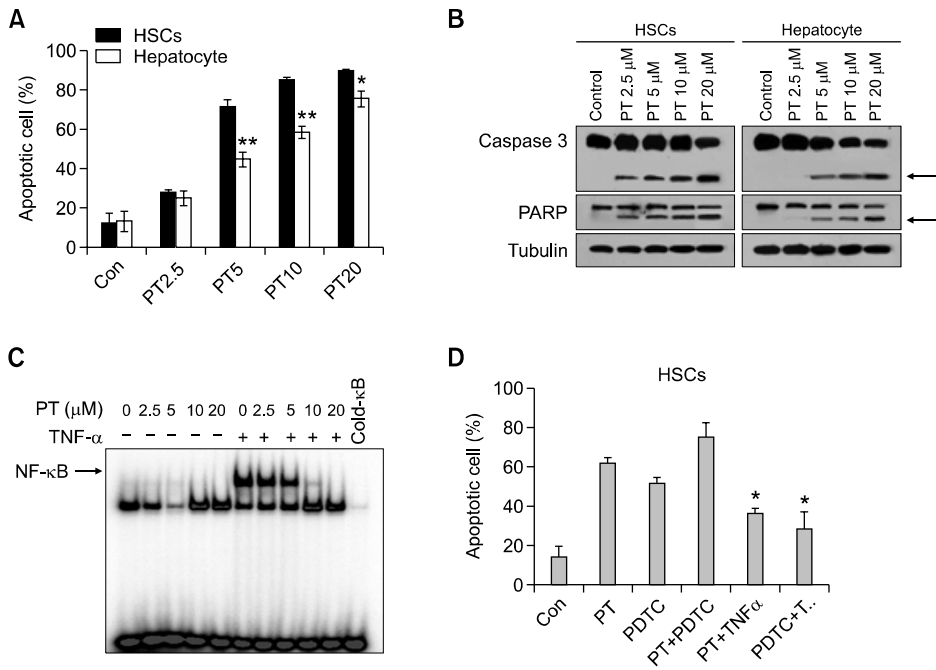

Figure 2. PT-induced apoptosis in HSCs and hepatocytes. (A) Effect of PT on the apoptotic cell death in primary HSCs and hepatocytes from rat liver tissue. **$P < 0.01$. *$P < 0.05$. (B) Western blot analysis demonstrated cleavage of PARP and caspase-3 in primary HSCs and hepatocytes treated with PT at indicated concentrations. (C) TNF-α-stimulated NF-κB binding activity in RI-T cells. TNF-α-stimulated (10 ng/ml) NF-κB binding activity was significantly suppressed by pretreatment with PT at 10-20 µM. (D) Effects of PT (10 µM) in combination with PDTC (100 µM) or TNF-α (10 ng/ml) on the apoptotic cell death in primary HSCs. *$P < 0.05$.
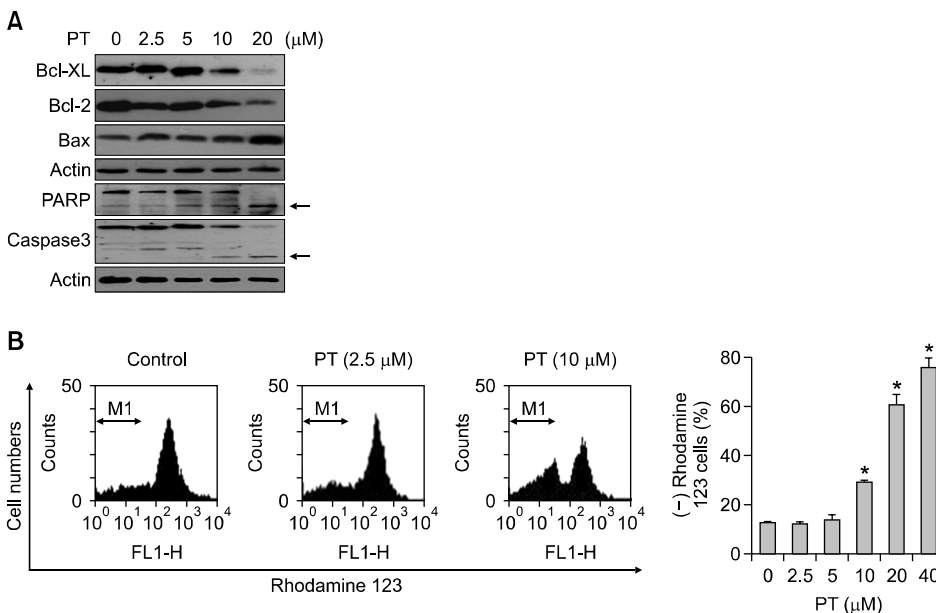

Figure 3. Effect of PT on the release of apoptosis-related proteins and MMP in RI-T cells. (A) Changes of Bcl-X$_L$, Bcl-2, and Bax expressions in RI-T cells treated with PT. (B) Cells stained with rhodamine 123 were counted with a FACStar flow cytometer. The graph shows percentages of rhodamine 123 negative cells. *$P < 0.05$ compared with the PT-untreated control group.
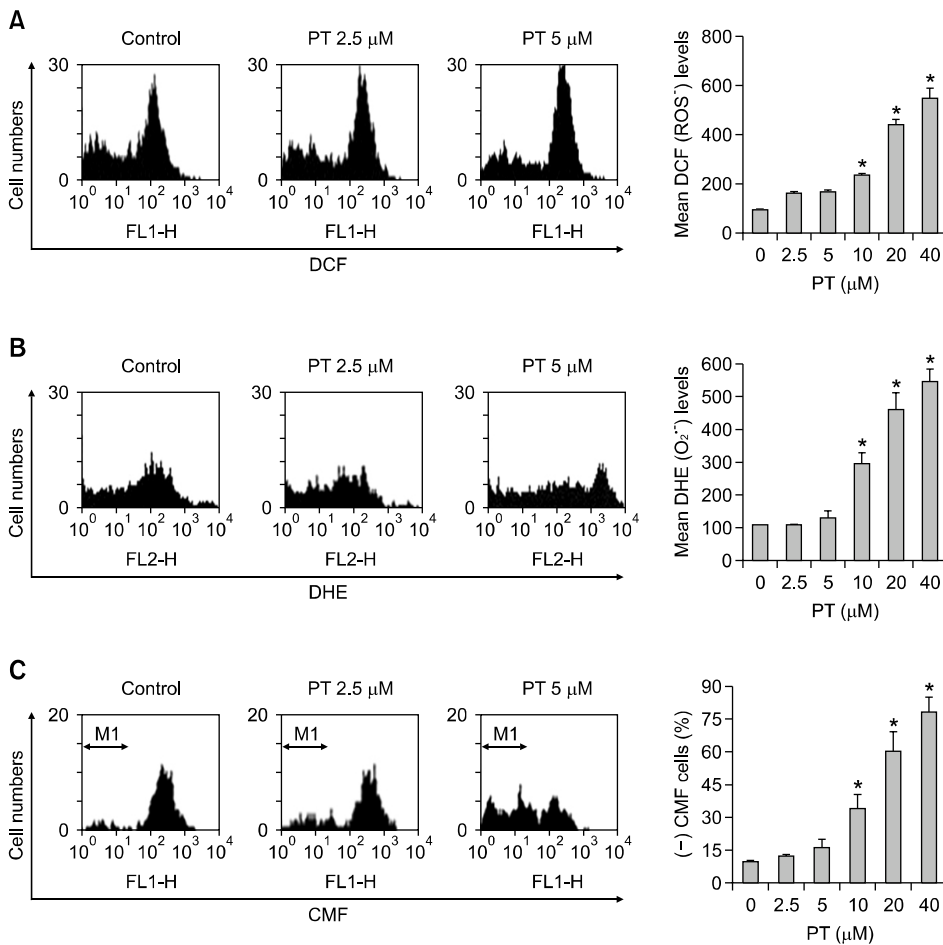
A

B

C

Figure 4. Increased intracellular oxidative stress in PT-treated RI-T cells. (A), (B) Intracellular ROS (DCF) and $O_2^{\bullet-}$ (DHE) levels in RI-T cells were measured using a FACStar flow cytometer. (C) Intracellular GSH levels. Graphs show levels of the mean DCF fluorescence of A, the DHE fluorescence of B, and the mean CMF fluorescence of C. *$P < 0.05$ compared with the control group.

of PARP were found to occur in a dose-dependent manner after 24 h. In addition, caspase-3 was activated in a dose-dependent manner, as demonstrated by a reduction in the levels of or cleavage of their pro-caspases (Figure 3A). Because it has been reported that apoptosis by PT is closely related to MMP collapse, we also investigated the effect of PT on MMP using rhodamine 123. Treatment with PT was found to induce a loss of MMP in RI-T cells after 24 h (Figure 3B). After exposure to 10 μM PT for 24 h, the percentage of MMP loss was approximately 77% compared with PT-untreated control cells.

Increased intracellular oxidative stress in relation to PT-induced apoptosis of rat HSCs

We investigated the effects of PT on intracellular ROS and GSH levels in RI-T cells. As shown in Figure 4A, ROS (DCF) levels were elevated in RI-T cells treated with PT at doses greater than 10 μM for 24 h. Levels of red fluorescence derived from DHE (reflecting $O_2^{\bullet-}$ accumulation) were unaltered in 2.5

or 5 μM PT-treated RI-T cells at 24 h. However, intracellular $O_2^{\bullet-}$ levels were markedly higher in 10, 20, and 40 μM PT-treated RI-T cells at 24 h ($P < 0.05$) (Figure 4B). We analyzed changes in GSH levels in RI-T cells using the fluorescent dye CMF. Treatment with PT increased the number of GSH-depleted RI-T cells dose-dependently (Figure 4C, $P < 0.05$). These results suggest that the pro-apoptotic activity of PT in RI-T cells is associated with increased intracellular oxidative stress.

Since PT was found to affect cell growth and the levels of intracellular ROS and GSH in RI cells, we assessed the effects of NAC and BSO on the growth and apoptosis of PT-treated RI-T cells. Exponentially growing cells were treated with 10 μM PT for 24 h following a 1 h pre-incubation with NAC or BSO. NAC (2 mM) significantly counteracted the growth-inhibiting effect of PT, whereas BSO (10 μM) further inhibited cell growth (Figure 5A). In addition, NAC decreased the percentage of annexin-V-positive cells among PT-treated RI-T cells, whereas BSO significantly increased the number of annexin

V-positive cells (Figure 5B). Next, we determined whether intracellular $O_2^{\bullet-}$ levels and GSH content in PT-treated RI-T cells were altered by treatment with NAC or BSO. Pretreatment with NAC (2 mM) reduced the PT-induced increase in intracellular $O_2^{\bullet-}$ levels and the number of GSH-depleted cells significantly, but BSO further increased intracellular $O_2^{\bullet-}$ levels and the number of GSH-depleted cells (Figure 5C and 5D).

Anti-fibrotic effects of PT in an *in vivo* rat model

The TAA group showed significant reduction in body and liver weight compared to the control group

Figure 5. Effects of NAC and BSO in PT-treated RI-T cells. (A) Cell growth inhibition was assessed using MTT assays. (B) Annexin-V-positive cell numbers were determined using a FACStar flow cytometer. Graphs show percentages of annexin-V-positive cells. (C) Intracellular $O_2^{\bullet-}$ (DHE) levels. (D) Intracellular GSH levels. Graphs show levels of the mean DHE fluorescence of C and of the mean CMF fluorescence of D. *$P < 0.05$ versus the control group. **$P < 0.05$ versus the PT 10 μM group.

(Table 1). In addition, the results of liver function tests indicated marked elevation of liver enzymes such as AST and ALT, and a decreased level of albumin in the TAA group compared to control group. Treatment with PT (2 mg/kg or 4 mg/kg) was found to restored these changes. Furthermore, treatment of these rats with PT (2 or 4 mg/kg) significantly ameliorated liver fibrosis as compared to the TAA group (Figure 6A, upper and middle panels). Immunohistochemical staining for α-SMA showed that its expression in the TAA group was significantly higher than in the control group (Figure 6A, lower panels). PT-treated (2 or 4 mg/kg) groups showed significantly lower α-SMA expression than the TAA group. When we assessed the stage of fibrosis and grade of lobular activity using Scheuer's scoring system, the PT-treated rats showed significantly less fibrosis and inflammatory activity, such as portal inflammation and intralobular degeneration, than the TAA-treated rats (Figure 6B). Furthermore, the PT treatment groups showed markedly lower levels of TGF-β1 expression than the TAA-treated model group (Figure 6C). To determine whether PT efficiently induced apoptotic cell death of HSCs in the livers of rats treated with TAA and PT4, we simultaneously analyzed terminal deoxynucleotidyl transferase dUDP nick-end labelling (TUNEL) positivity and HSC-specific glial fibrillary acidic protein (GFAP) immunostaining. Our data showed that TUNEL-positive cells were also positive for GFAP (Figure 6D). These resuls suggests that PT could induce apoptotic cell death in activated hepatic stellate cells by TAA.
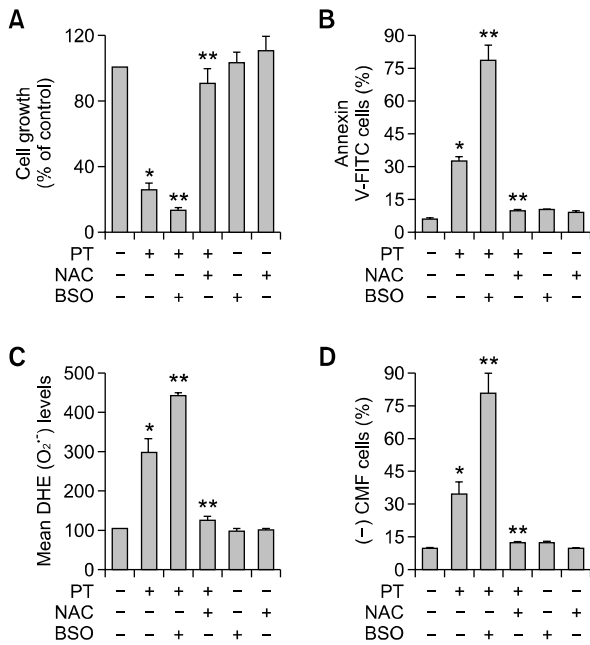
Discussion

In this study, we demonstrate the apoptotic effects of PT in RI-T cells as well as rat hepatic HSCs. Consistent with similar studies in cancer cell lines, we found that PT inhibits cell growth and induces apoptotic cell death in a dose-dependent manner in HSCs. These effects were associated with the inhibitory effect on TNF-α-stimulated NF-κB binding activity, activation of caspase-3, PARP cleavage,

Table 1. Body weights, liver weights, and liver function test results

Group	Body weight (g)	Liver weight (g)	ALT (IU/L)	AST (IU/L)	Albumin (g/dL)
Control	443.3 ± 60.4	15.2 ± 2.0	35.5 ± 6.5	106.8 ± 16.7	4.0 ± 0.1
TAA	292.8 ± 17.7*	11.8 ± 0.6*	181.0 ± 105.6*	421.2 ± 178.0*	3.7 ± 0.3*
TAA + PT2	334.7 ± 15.0**	13.1 ± 1.0**	62.7 ± 21.6**	116.8 ± 35.8**	4.0 ± 0.6**
TAA + PT4	336.7 ± 17.8**	13.6 ± 1.1**	50.5 ± 8.4**	109.3 ± 26.1**	4.1 ± 0.6**

TAA, thioacetamide; PT2, parthenolide 2 mg/kg; PT4, parthenolide 4 mg/kg.
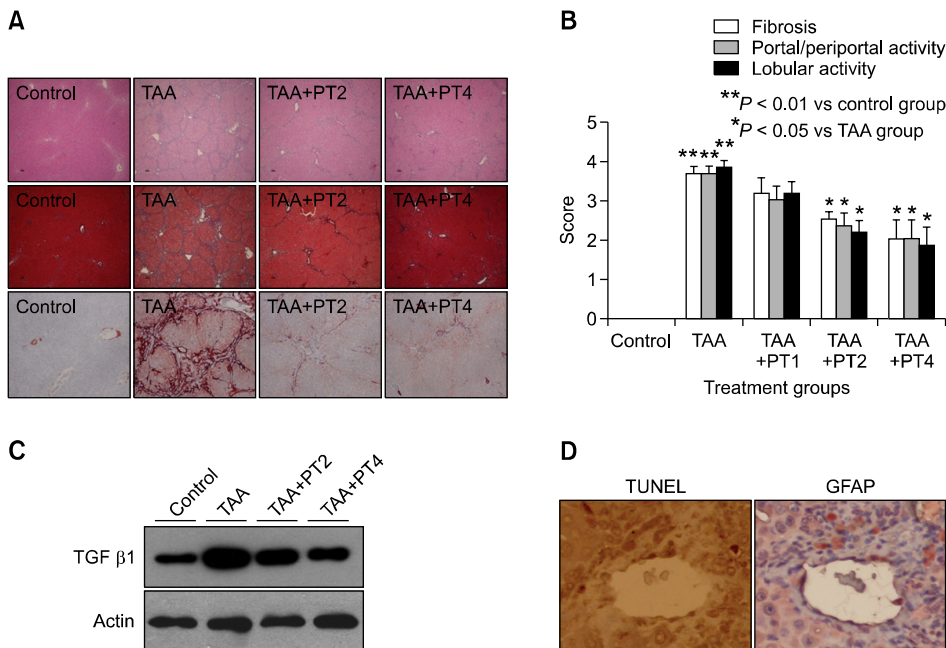*$P < 0.05$ versus the control group. **$P < 0.05$ versus the TAA group.

A

B

C

D

Figure 6. Anti-fibrotic effects of PT in TAA-treated rats. (A) Representative microscopic images of rat liver, hematoxylin and eosin staining (upper panels), Masson-trichrome stain (middle panels), and immunohistochemical staining for α-SMA in rat liver (lower panels). (B) Histopathologic score obtained using Scheuer's scoring system as described in the 'Materials and Methods'. Treatment groups: I, control; II, TAA; III, TAA+PT2; IV, TAA+PT4. (C) PT inhibited TAA-induced TGF-β1 expression as shown by Western blot analysis. TAA, thioacetamide; PT2, parthenolide 2 mg/kg; PT4, parthenolide 4 mg/kg. (D) TUNEL staining and GFAP immunostaining showed co-localization of TUNEL positives and GFAP immunoreactivities in hepatic HSCs from the liver tissue of rats treated with TAA and PT4 ($\times$ 400).

the modulation of Bcl-2 family proteins, increased intracellular ROS levels, and depletion of intracellular GSH levels. Furthermore, PT ameliorated hepatic fibrosis in an *in vivo* rat model. This apoptotic effect of PT was significantly higher in HSCs than in hepatocytes.

Several studies have provided indirect evidence of an anti-apoptotic role played by NF-κB in HSCs (Saile *et al.*, 2001, 2004; Oakley *et al.*, 2003). More recent *in vitro* and *in vivo* studies have provided definitive evidence of the protective role played by NF-κB in HSC apoptosis (Oakley *et al.*, 2005). Previous studies have described PT as a potent inhibitor of NF-κB. According to numerous findings, PT inhibits IκB kinase complex, which results in the sustained cytoplasmic retention of NF-κB (Hehner *et al.*, 1999; Kwok *et al.*, 2001; Saadane *et al.*, 2007). Consequently, a lack of NF-κB activity renders cancer cells prone to undergoing apoptosis or sensitizes them to cytokine- or anti-cancer drug-induced cell death (Zhang *et al.*, 2004a). In this study, PT had a strong inhibitory effect on TNF-α stimulated NF-κB binding activity in rat HSCs. We speculate that this effect contributes to the anti-proliferative and pro-apoptotic efficacy of PT in HSCs. Another NF-κB inhibitor, PDTC, also showed the same apoptogenic effect.

With respect to the molecular mechanism underlying PT-induced apoptosis, we found that apoptotic induction was accompanied by the upregulation of the Bax protein and the downregulation of the Bcl-2 and Bcl-X$_L$ proteins. It has been suggested that a high Bax to Bcl-2 ratio can cause MMP collapse and

result in the release of cytochrome c and subsequent apoptosis (Yang *et al.*, 1997). Likewise, the high ratio of Bax to Bcl-2 in PT-treated HSCs probably damaged the mitochondrial membrane and triggered MMP collapse. Consequently, the loss of MMP may cause the release of pro-apoptotic inducers, such as cytochrome c, HtrA2, Samc/Diablo, or AIF, which induce apoptosis *via* the activation of caspases. It is worth noting that there were similar levels of annexin-V-positive and rhodamine-123-negative cells, which suggests that apoptosis is tightly related to or dependent on the loss of MMP.

The redox state of cells has been shown to be involved in cell cycle regulation and cell death/survival (Schumacker, 2006). In a previous study using human HSCs, it was suggested that oxidative stress is a requirement for cell killing by gliotoxin (Kweon *et al.*, 2003). In the present study, PT induced apoptotic cell death *via* the formation of ROS. According to our results, intracellular ROS levels, especially O$_2^{\bullet-}$, were significantly elevated in rat HSCs treated with PT. GSH is the main intracellular antioxidant and plays an important role in these processes; whereas GSH depletion causes cell death (Oakley *et al.*, 2005), an increase in GSH inhibits cell proliferation (Menon *et al.*, 2003). In the present study, PT dose-dependently increased the number of GSH-depleted cells. Furthermore, NAC (a GSH precursor) significantly reduced the number of GSH-depleted cells and abrogated apoptotic cell death in PT-treated rat HSCs. In contrast, BSO (a glutathione depleting agent) augmented the number of GSH-depleted cells and increased apoptotic cell

death among PT-treated HSCs. Taken together these results suggest that an increase in oxidative stress is involved in PT-induced apoptosis of HSCs.

Furthermore, through improved histopathological findings we also demonstrated that PT (at 2 and 4 mg/kg) significantly reduced hepatic fibrosis in TAA-treated rats and decreased expression of TGF-β1. PT also reduced the expression of α-SMA as assessed by immunohistochemistry, which suggests that there was a decrease in the number of activated HSCs.

In conclusion, PT has potent anti-fibrotic activity both *in vitro* and *in vivo*. Although PT has been actively investigated as an anti-inflammatory or anti-cancer drug for many yr, our findings suggest that its efficacy and mechanism of preventing or regressing liver fibrosis should be further explored. The present study enhances our understanding of the anti-fibrotic efficacy of PT by demonstrating that PT induces apoptotic cell death in rat HSCs *via* an increase in intracellular oxidative stress and inhibition of TNF-α-stimulated NF-κB binding activity and also by showing that PT ameliorates hepatic fibrosis in an *in vivo* model.

Methods

Cell culture and reagents

RI-T cells (Health Science Research Resources Bank; HSRRB, JCRB1088, Osaka, Japan), a previously described immortalized rat hepatic stellate cell line (Tokiwa *et al.*, 1999), were used in the present study. Cells were cultured in Dulbecco's modified Eagle's medium (GibcoBRL, Grand Island, NY) supplemented with 10% fetal bovine serum and standard antibiotics in a 95% air, 5% CO_2 humidified atmosphere at 37°C. Primary hepatic stellate cells (HSCs) and hepatocytes were simultaneously isolated from rat liver tissue and cultured as previously described (Riccalton-Banks *et al.*, 2003).

PT was purchased from Calbiochem (San Diego, CA) and dissolved in ethanol to make a 40 mM stock solution. N-acetyl-cysteine (NAC) and L-buthionine sulfoxamine (BSO) were obtained from Sigma-Aldrich (St. Louis, MO). NAC was dissolved in a buffer (20 mM HEPES [pH 7.0]) and BSO was dissolved in ethanol to make 100 mM stock solutions. Ethanol (0.2%) was used as a control vehicle, and at this level did not affect cell growth or death. PDTC and TNF-α were obtained from Sigma Co. (Saint Louis, MO).

Cell growth inhibition and apoptosis assays

After treatment with the indicated concentrations (0, 2.5, 5, 10, 20, 40 μM) of PT or vehicle for 24 h, cell growth inhibition was determined using a 3-(4,5-dimethylthiazol-2-yl)-2,5-diphenyltetrazolium bromide (MTT) dye absorbance assay. Cell cycle and sub-G1 distribution was analyzed using a FACStar flow cytometer (Becton Dickinson, San Jose, CA). Apoptosis was determined by staining cells

with annexin V-fluorescein isothiocyanate (FITC, PharMingen, San Diego, CA; Ex/Em = 488 nm/519 nm) and PI labeling. Mitochondrial membrane potential (MMP) was monitored using the fluorescent dye rhodamine 123 (Sigma-Aldrich; Ex/Em = 485 nm/535 nm). The terminal deoxynucleotidyl transferase biotin-dUTP nick end labeling (TUNEL) assay was done according to the manufacturer's protocol (Chemicon, Temecula, CA).

Electrophoretic mobility shift assays for NF-κB binding activity

For TNF-α stimulation experiments, RI-T cells (1×10^6 cells) were pretreated with the indicated concentrations of PT for 12 h and then incubated with or without TNF-α (10 ng/ml; R & D Systems, Minneapolis, MN) for 30 min. Cells were immediately washed twice, scraped into 1.5 mL of ice-cold PBS (pH 7.9), and pelleted at $12,000 \times g$ for 30 s. Cytoplasmic and nuclear extracts were prepared using NE-PER Nuclear and Cytoplasmic Extraction Reagents (Pierce Biotechnology, Rockford, IL). NF-κB activation was assessed using a gel mobility shift assay using nuclear extracts.

Western blot analysis

Cells were incubated with the designated doses of PT for 24 h, washed in PBS, and suspended in 5 volumes of lysis buffer (20 mM HEPES [pH 7.9], 20% glycerol, 200 mM KCl, 0.5 mM EDTA, 0.5% NP40, 0.5 mM DTT, 1% protease inhibitor cocktail) (Sigma). Supernatant protein concentrations were determined using the Bradford method. Supernatant samples containing 40 μg of total protein were resolved using 10-15% SDS-PAGE gels and transferred onto Immobilon-P PVDF membranes (Millipore, Billerica, MA) by electroblotting. Samples were then probed with anti-α-SMA, anti-Bax, anti-Bcl-2, anti-Bcl-X_L, anti-caspase-3, anti-poly-(ADP-ribose)-polymerase (PARP), anti-GFAP (Millipore), and anti-actin (Santa Cruz Biotechnology, SantaCruz, CA) antibodies. The membranes were incubated with horseradish peroxidase-conjugated secondary antibodies, and blots were developed using the ECL kit (Amersham, Arlington Heights, IL).

Determination of intracellular ROS and glutathione (GSH) levels

Intracellular ROS, such as, $H_2O_2^{\bullet-}$, $^\bullet OH$, and $ONOO^\bullet$, were detected using an oxidation sensitive fluorescent probe dye, 2',7'-dichlorodihydrofluorescein diacetate (H_2DCFDA, Invitrogen Molecular Probes, Eugene, OR; Ex/Em = 495 nm/529 nm) (Kim *et al.*, 2008). Because H_2DCFDA is only poorly selective for $O_2^{\bullet-}$, dihydroethium (DHE, Invitrogen Molecular Probes; Ex/Em = 518 nm/605 nm) was used to detect $O_2^{\bullet-}$. DCF and DHE fluorescence was detected using a FACStar flow cytometer (Becton Dickinson). ROS and $O_2^{\bullet-}$ levels are expressed as mean fluorescent intensities (MFIs), which were calculated using CellQuest software (Becton Dickinson). Cellular GSH levels were analyzed using the membrane permeable dye 5-chloromethylfluorescein (CMFDA, Invitrogen Molecular Probes;

Ex/Em = 522 nm/595 nm). Cytoplasmic esterases convert CMFDA to fluorescent 5-chloromethylfluorescein, which can then react with GSH. CMF fluorescence intensities were determined using a FACStar flow cytometer (Becton Dickinson). Cells negative for CMF staining (GSH depleted) are expressed as percentages of total cells.

In vivo rat hepatic fibrosis model

Male Sprague-Dawley (180-200 g) rats (Charles River Laboratories, Yokohama, Japan) were provided a standard laboratory diet and water *ad libitum*. TAA was purchased from Sigma-Aldrich. Hepatic fibrosis was induced by injecting TAA (200 mg/kg body weight, i.p.) three times a week for 8 weeks. Our experiment included five groups. The control group received only vehicle for 8 weeks. After 6 weeks of TAA injections, rats were randomly divided into groups as follows. TAA group received an equal volume of DMSO (vehicle of PT) in 200 μl saline i.p. three times a week 1 h before TAA for 2 weeks. TAA+PT2 and TAA+PT4 groups received PT (2 mg/kg, and 4 mg/kg body weight, i.p., respectively) three times a week 1 h before the TAA injections for 2 weeks. Each group contained 6 rats. Animals were anesthetized with ether at the end of treatment and their body weights were recorded. Blood samples were obtained for testing liver functions. Alanine aminotransferase (ALT), aspartate aminotransferase (AST), and albumin in plasma were analyzed using an automatic blood chemistry analyzer (Abbott Laboratories, Abbott Park, IL). All animal experiments were performed in accordance with specific permissions issued by the institutional board of animal care and use committee of Chonbuk National University Medical School.

Histochemical staining of formalin-fixed liver sections with hematoxylin and eosin (HE) or Masson's trichrome and immunohistochemical staining for α-SMA were performed. Pathological scoring was performed by two blinded independent pathologists using Scheuer's scoring system (Scheuer, 1991). Fibrosis was staged as follows: stage 0, no fibrosis; stage 1, expansion of the portal tract without linkage; stage 2, periportal or portal to portal septa but intact architecture; stage 3, fibrosis with architectural distortion but no obvious cirrhosis, and stage 4, cirrhosis. Portal/periportal activity was graded as follows: grade 0, none or minimal; grade 1, portal inflammation; grade 2, mild piecemeal necrosis; grade 3, moderate piecemeal necrosis; and grade 4, severe piecemeal necrosis. Lobular activity was graded as follows: grade 0, none; grade 1, inflammation but no necrosis; grade 2, focal necrosis or acidophil bodies; grade 3, severe focal cell damage; and grade 4, damage including bridging necrosis. Liver samples were homogenized in 500 mmol/L Tris buffer (pH 7.6) containing 1% Triton X-100, 200 mmol/L NaCl, and 10 mmol/L $CaCl_2$. After centrifugation at 14,000 *g* at 4°C for 30 min, supernatants were assayed for TGF-β1 activity by immunoblotting as described above.

Statistical analysis

The results represent the mean of at least three independent experiments (mean ± SD). Data were analyzed using Instat software (GraphPad Prism4, San Diego, CA).

Student's *t*-test or one-way ANOVA with post hoc analysis using Tukey's multiple comparison test were used to analyze parametric data. Statistical significance was accepted for *P* values < 0.05.

References

Arthur MJ. Reversibility of liver fibrosis and cirrhosis following treatment for hepatitis C. Gastroenterology 2002;122:1525-8

Elsharkawy AM, Oakley F, Mann DA. The role and regulation of hepatic stellate cell apoptosis in reversal of liver fibrosis. Apoptosis 2005;10:927-39

Friedman SL. Molecular regulation of hepatic fibrosis, an integrated cellular response to tissue injury. J Biol Chem 2000;275:2247-50

Habens F, Srinivasan N, Oakley F, Mann DA, Ganesan A, Packham G. Novel sulfasalazine analogues with enhanced NF-κB inhibitory and apoptosis promoting activity. Apoptosis 2005;10:481-91

Hehner SP, Heinrich M, Bork PM, Voqt M, Ratter F, Lehmann V, *et al*. Sesquiterpene lactones specifically inhibit activation of NF-kappa B by preventing the degradation of I kappa B-alpha and I kappa-beta. J Biol Chem 1998;273:1288-97

Hehner SP, Hofmann TG, Droge W, Schmitz ML. The anti-inflammatory sesquiterpene lactone parthenolide inhibits NF-κB by targeting the IκB kinase complex. J Immunol 1999; 163:5617-23

Iredale JP, Benyon RC, Pickering J, McCullen M, Northrop M, Pawley S, *et al*. Mechanisms of spontaneous resolution of rat liver fibrosis. Hepatic stellate cell apoptosis and reduced hepatic expression of metalloproteinase inhibitors. J Clin Invest 1998;102:538-49

Kim SW, Han YW, Lee ST, Jeong HJ, Kim SH, Kim IH, *et al*. A superoxide anion generator, pyrogallol, inhibits the growth of HeLa cells via cell cycle arrest and apoptosis. Mol Carcinog 2008;47:114-25

Kweon YO, Paik YH, Schnabl B, Qian T, Lemasters JJ, Brenner DA. Gliotoxin-mediated apoptosis of activated human hepatic stellate cells. J Hepatol 2003;39:38-46

Kwok BH, Koh B, Ndubuisi MI, Elofsson M, Crews CM. The anti-inflammatory natural product parthenolide from the medical herb Feverfew directly binds to and inhibits IkappaB kinase. Chem Biol 2001;8:759-66

Menon SG, Sarsour EH, Spitz DR, Higashikubo R, Sturm M, Zhang H, *et al*. Redox regulation of the G1 to S phase transition in the mouse embryo fibroblast cell cycle. Cancer Res 2003;63:2109-17

Montiel-Duarte C, Ansorena E, López-Zabalza MJ, Cenarruzabeitia E, Iraburu MJ. Role of reactive oxygen species, glutathione and NF-κB in apoptosis induced by 3,4-methylenedioxymethamphetamine ("Ecstasy") on hepatic stellate cells. Biochem Pharmacol 2004;67:1025-33

Oakley F, Meso M, Iredale JP, Green K, Marek CJ, Zhou X, *et al*. Inhibition of inhibitor of kappaB kinases stimulates hepatic stellate cell apoptosis and accelerated recovery from rat liver fibrosis. Gastroenterology 2005;128:108-20

Oakley F, Trim N, Constandinou CM, Ye W, Gray AM, Frantz G, *et al*. Hepatocytes express nerve growth factor during liver injury. Am J Pathol 2003;163:1849-58

Pajak B, Gajkowska B, Orzechowski A. Molecular basis of parthenolide-dependent proapoptotic activity in cancer cells. Folia Histochem Cytobiol 2008;46:129-35

Riccalton-Banks L, Bhandari R, Fry J, Shakesheff KM. A simple method for the simultaneous isolation of stellate cells and hepatocytes from rat liver tissue. Mol Cell Biochem 2003;248:97-102.

Saadane A, Masters S, DiDonato J, Li J, Berger M. Parthenolide inhibits IkappaB kinase, NF-κB activation and inflammatory response in cystic fibrosis cells in mice. Am J Respir Cell Mol Biol 2007;36:728-36

Saile B, DiRocco P, Dudas J, El-Armouche H, Sebb H, Eisenbach C, *et al*. IGF-I induces DNA synthesis and apoptosis in rat liver hepatic stellate cells (HSC) but DNA synthesis and proliferation in rat liver myofibroblasts (rMF). Lab Invest 2004;84:1037-49

Saile B, Matthes N, El Armouche H, Neubauer K, Ramadori G. The blc, NFkappaB and p53/p21WAF1 systems are involved in spontaneous apoptosis and in the anti-apoptotic effect of TGF-beta and TNF-alpha on activated hepatic stellate cells. Eur J Cell Biol 2001;80:554-61

Scheuer PJ. Classification of chronic viral hepatitis: a need for reassessment. J Hepatol 1991;13:372-4

Schinella GR, Giner RM, Recio MC, Mordujovich de Buschiazzo P, Ríos JL, Máñez S. Anti-inflammatory effects of South American Tanacetum vulgare. J Pharm Pharmacol 1998;50:1069-74

Schumacker PT. Reactive oxygen species in cancer cells: live by the sword, die by the sword. Cancer Cell 2006;10:175-6

Tokiwa T, Yata Y, Takahara T, Watanabe A, Enosawa S, Suzuki S, *et al*. SV40 large T antigen immortalization of rat hepatic stellate-like cells. *In Vitro* Cell Dev Biol Anim 1999;35:246-7

Wang W, Adachi M, Kawamura R, Sakamoto H, Hayashi T, Ishida T, *et al*. Parthenolide-induced apoptosis in multiple myeloma cells involves reactive oxygen species generation and cell sensitivity depends on catalase activity. Apoptosis 2006;11:2225-35

Wen J, You KR, Lee SY, Song CH, Kim DG. Oxidative stress-mediated apoptosis. The anticancer effect of the sesquiterpene lactone parthenolide. J Biol Chem 2002;277:38954-64

Yang J, Liu X, Bhalla K, Kim CN, Ibrado AM, Cai J, *et al*. Prevention of apoptosis by Bcl-2: Release of cytochrome c from mitochondria blocked. Science 1997;275:1129-32

Zhang S, Lin ZN, Yang CF, Shi X, Ong CN, Shen HM. Suppressed NF-κB and sustained JNK activation contribute to the sensitization effect of parthenolide to TNF-α-induced apoptosis in human cancer cells. Carcinogenesis 2004a;25:2191-9

Zhang S, Ong CN, Shen HM. Critical roles of intracellular thiols and calcium in parthenolide-induced apoptosis in human colorectal cancer cells. Cancer Lett 2004b;208:143-53